LA-UR-99-3287
Approved for public release;
distribution is unlimited.

Title: **Results from LSND on Neutrino Physics**

Author(s): Geoffrey B. Mills

Submitted to:

http://lib-www.lanl.gov/la-pubs/00796661.pdf

Results from LSND on Neutrino Physics

Geoffrey B. Mills
(Representing the LSND Collaboration[1])
Physics Division
Los Alamos National Laboratory
Los Alamos, NM 87545
USA
e-mail: mills@lanl.gov

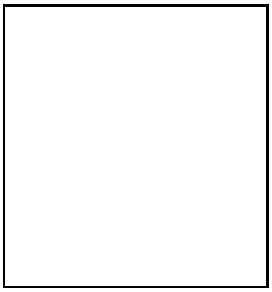

The LSND collaboration has searched for neutrino oscillations in neutrinos produced at the LANSCE facility at the Los Alamos National Laboratory. The collaboration finds an excess of events consistent with $\bar{\nu}_\mu \to \bar{\nu}_e$ oscillations. The excess of events from all runs (1993-1998) is consistent with $\nu_\mu \to \nu_e$ oscillations. An excess of 111.7 ± 25.6 events is observed with e^+ energy between 20 and 60 MeV for the $\bar{\nu}_\mu \to \bar{\nu}_e$ search. For the $\nu_\mu \to \nu_e$ search, an excess of $18.1 \pm 6.6 \pm 4.0$ events is observed with e^- energy between 60 and 200 MeV.

1 Overview

The search for a signature of finite mass in the neutrino sector has been long, diffucult, and challenging. In order to establish that neutrinos have non-zero mass, one is required either to measure the mass directly, e.g. via conservation of energy, or to show that neutrinos oscillate with a mass-like phase advance. The phase advance in the latter case must be proportional to the difference in proper times of the neutrino eigenstates. Neutrino oscillations not only require massive neutrinos, they also require the neutrino mass eigenstates to be mixed. Neutrinos can mix in several possible ways, with non-interacting chiral partner states (sterile neutrinos), with different generation flavor states, or with a combination of these. The sterile oscillations are observed only in disappearance experiments while flavor oscillations can be observed in both disappearance and in appearance experiments.

There are three well known experimental hints of neutrino mass, all having to do with the observation of neutrino oscillations. The deficits of solar ν_e neutrinos and atmospheric ν_μ neutrinos are well documented disappearance results. In these results, the phase dependence seems to be observed however one cannot yet distinguish between sterile and flavor oscillations.

The third hint of neutrino mass is the observed anomalous appearance of $\bar{\nu}_e$ and ν_e by the LSND collaboration [2,3]. The phase dependence in this case has not yet been verified, however, oscillations remain the favored explanation of the anomaly. That result is the subject of this manuscript.

2 The LSND Experiment

The technique employed by LSND to observe neutrino oscillations is an appearance experiment. A beam of neutrinos is prepared at a beam dump, and the flavor composition of the beam is observed some distance away from the production source. An excess of any type of neutrino above calculated rates indicates a change in in the flavor composition and indicate that oscillations may have occurred.

The LANSCE linear accelerator produces a beam a 200 MHz RF micro structure, on top of a 120 Hz macro-pulse structure. The macro-pulses are roughly 700 μs long, that gives a duty ratio of 5-8% for normal running. The data between macro pulses serves to measure random cosmic ray backgrounds.

For LSND, the 1 mA beam of protons from the linear accelerator impacts upon a beam dump to produce charged pions. These pions either decay in flight, decay at rest, or (in the case of negative pions) are absorbed on nuclei in the dump. The neutrinos produced in those decays escape, and the resulting muons either decay , or (in the case of negative muons) undergo conversion on a nucleus in the beam dump. This sequence of decays produces a beam of neutrinos in the LSND detector. The composition of the beam dump has been varied over the course of the LSND running from a low Z water target to a high Z tungsten target with no significant effect on the rate of anomalous events. Careful simulations of the beam dump area are used to calculate expected neutrino fluxes [4].

The neutrino composition in such a beam is ideal for $\bar{\nu}_e$ appearance experiments. There are eight times as many positive pions produced as negative pions. Only five percent of those negative pions decay, and of those negative muons that result, only twelve percent decay. The ratio of negative muon decays to positive muon decays is thus less than 7.5×10^{-4}. The appearance of excess $\bar{\nu}_e$ is observable above this level.

At energies above the muon decay endpoint the pion decay-in-flight neutrinos dominate the flux. The appearance of excess ν_e is then observable since normal decay channels are suppressed by the low (1.2×10^{-4}) branching ratio and by the long lifetime of the daughter muon relative to the flight time of the muon (5.0×10^{-4}).

The fluxes are calculated by using code[4] that simulates the beam stop geometry, materials, and particle production. The code was calibrated by using a test beam setup which was sensitive to pion production from 800 MeV protons. The systematic error on the decay-at-rest flux is found to be seven percent and the systematic error on the decay-in-fight flux is found to be fifteen percent.

3 Experimental Apparatus and Neutrino Detection

The LSND detector[5] consists of a cylindrical tank filled with 167 tons of active mineral oil target fluid. The fluid is composed of hydrocarbon chains of roughly 25 carbon units with a CH_2 stoichiometry. A small amount (0.031 g/l) of butyl-PBD is added to the oil in order to enhance the production of scintillation light in the fluid. This low scintillator concentration allows the detection of both Čerenkov light and scintillation light and yields a relatively long attenuation length of more than 20 m for wavelengths greater than 400 nm[6]. A typical 45 MeV electron created in the detector produces a total of around 1500 photoelectrons, of which around 280 photoelectrons are in the Čerenkov cone.

This fluid is viewed by 1220 8-inch photo-multiplier tubes mounted on the inner surface of the tank. The tubes achieve a 25 percent coverage with a quantum efficiency of 25 percent. The electronic readout of those tubes yields both photon arrival time and charge information for each tube.

Neutrinos interact with the carbon nuclei, hydrogenic protons, and electrons inside the tank volume. The daughter products of these reactions produce light inside the tank. The timing and charge information is then used to reconstruct the position, time, and direction of the event. Calibration of the system is achieved by using a large sample of electrons and positrons from the decay of stopped cosmic-ray muons.

Relativistic particles produce both Čerenkov light and isotropic scintillation light. The former is emitted in a characteristic Čerenkov cone at an angle of 47 degrees. More than half of the Čerenkov light is isotropically scattered by the fluid due to the presence of the scintillation fluor in the liquid. The Čerenkov light is produced almost immediately while the scintillation light has a exponential decay time of roughly 30 ns. Non-relativistic particles produce only scintillation light and can be separated from relativistic particles by analyzing the time distribution of the detected light and by the presence of a Čerenkov cone in the angular distribution of the light.

The detector tank is surrounded by a veto shield[7] which is used to suppress cosmic ray muon events at the trigger level. Trigger activities inhibit the trigger for 15.0 μs subsequent to the activity. This reduces the trigger rate to less than 50 Hz at the expense of a 19% loss in detector live time.

The detector trigger runs on a 100ns clock and the number of PMT's are summed every 100ns. Threshold levels of 18, 21, 75, and 150 hit PMT's for tank hits, and 4 or 6 hit PMT's for veto hits are recorded in a time stamped trigger word at every clock edge. A trigger processor then reads these words and decides whether or not an interesting event has occurred. If an interesting event is found, the trigger processor signals readout processors to send the event to the online reconstruction computer, which reconstructs the event and records it on tape. The trigger processor also watches for 1000 μs subsequent to the event and sends any events which might be 2.2 MeV gamma candidates in that interval. All activities which occur within 50 μs prior to the trigger event are also recorded. The trigger operates almost independently of whether the beam is on or off.

4 Neutrino Cross Section Measurements

There are several neutrino cross sections which have been measured by LSND. These events may also be used to cross check the calculated neutrino fluxes used in the oscillation searches. They arise from the interactions of the dominant neutrino components in the beam, ν_e from μ^+ decay at rest (DAR), and, ν_μ from pion decay in flight (DIF).

The μ^+ decay at rest neutrinos have energies below the muon rest mass, so only the ν_e can interact via a charged current reaction on the neutrons inside a carbon nucleus, ($^{12}C(\nu_e, e^-)\ ^{12}N$). There are two categories for this reaction. They are distinguished by the whether the resulting ^{12}N nucleus is in its ground state or not. The ground state ^{12}N nucleus will β decay back to the original ^{12}C configuration with a lifetime of 15.9 ms ($^{12}C(\nu_e, e^-)\ ^{12}N$). This signature is observable in the detector as an event correlated in position and time with the neutrino event. The presence of the correlated β decay event serves to reduce random backgrounds to this process. In addition, the nuclear matrix element for the neutrino cross section is directly related to the β decay matrix element, which is well measured. Thus, the number of observed ground state events is an accurate measure of

the decay-at-rest (DAR) flux.

In the case where the ν_e interaction leaves the ^{12}N nucleus in an excited state, ($^{12}C(\nu_e, e^-)\ ^{12}N^*$), it is well known that the excited nitrogen nucleus will decay via proton emission without returning to its ground state. Therefore no subsequent correlated β decay will be observed.

The energies of the pion decay-in-flight neutrinos extend above the threshold for muon production on carbon of 123.1 MeV, so that the $^{12}C(\nu_\mu, \mu^-)\ ^{12}N$ cross sections are measurable. These reactions are also coincidence measurements in the sense that the subsequent decay of the muon and/or β decay is correlated to the neutrino interaction in position and time. They have low accidental backgrounds. The matrix element for the $^{12}C(\nu_\mu, \mu^-)\ ^{12}N_{GS}$ reaction is well determined by the $^{12}N_{GS}$ lifetime, however, the statistics are poor. The calculations of the $^{12}C(\nu_\mu, \mu^-)\ ^{12}N^*$ cross sections are less certain. CRPA and shell model predictions range widely, and, for the moment, the measured rate is below the predicted values, although only slightly below the shell model predictions.

The ν_e, $\bar{\nu}_\mu$, and ν_μ can both interact with the electrons in the tank fluid, and, in the case of the ν_e, via both the s-channel and t-channel paths. These events are peaked forward in the angle with respect to the neutrino direction, and they can be distinguished from nuclear scattering processes.

The LSND measurements[8,9] of these cross sections are shown in Table 1. The ground state reaction measurements ($^{12}C(\nu_e, e^-)\ ^{12}N_{GS}$ and $^{12}C(\nu_\mu, \mu^-)\ ^{12}N_{GS}$) agree well with theoretical predictions and lend confidence to the flux calculations. The $^{12}C(\nu_e, e^-)\ ^{12}N^*$ and νe^- reactions agree well with theory.

The $^{12}C(\nu_\mu, \mu^-)\ ^{12}N$ inclusive cross section is complicated by the nuclear dynamics of the $^{12}N^*$ system since the momentum transfer is larger than in the case of the $^{12}C(\nu_e, e^-)\ ^{12}N$. The CRPA model calculations[10] have been unable to reproduce the LSND measured values. The situation has been nearly resolved because of two new revelations. Improvements in our flux calculations have raised slightly the LSND measured value. Recent shell model calculations[12] yield a smaller number than the CRPA model. Correlations in the closed $p_{3/2}$ shell nucleons seem to have a larger effect than previously assumed, so that the theory is more compatible with the LSND results.

Table 1: Summary of LSND Cross Section Measurements

Process	Measured	Prediction	Neutrino Source
$^{12}C(\nu_e, e^-)\ ^{12}N_{GS}$	$(9.1 \pm 0.4 \pm 0.9) \times 10^{-42}$	9.3×10^{-42}	μ^+ decay at rest
$^{12}C(\nu_e, e^-)\ ^{12}N^*$	$(5.7 \pm 0.6 \pm 0.6) \times 10^{-42}$	6.3×10^{-42}	μ^+ decay at rest
νe^-	$(4.2 \pm 0.6 \pm 0.4) \times 10^{-42}$	3.97×10^{-42}	μ^+ decay at rest
$^{12}C(\nu_\mu, \mu^-)\ ^{12}N_{GS}$	$(6.6 \pm 1.1 \pm 1.0) \times 10^{-41}$	6.4×10^{-41}	π^+ decay in flight
$^{12}C(\nu_\mu, \mu^-)\ ^{12}N$	$(12.3 \pm 0.3 \pm 1.8) \times 10^{-40}$	$(13 - 20) \times 10^{-40}$	π^+ decay in flight

5 Neutrino Oscillations

LSND has performed searches for signs of neutrino oscillations in two separate channels. The decay at rest flux is ideal for studying the $\bar{\nu}_\mu \to \bar{\nu}_e$ transition and the decay at rest flux is suited to study the $\nu_\mu \to \nu_e$ transition. In either case, a search for events with an event with and electron-like signature(positrons behave identically to electrons in LSND).

5.1 $\bar{\nu}_\mu \to \bar{\nu}_e$ Ocillations

The $\bar{\nu}_\mu \to \bar{\nu}_e$ relies on the absence of $\bar{\nu}_e$ in the initial neutrino beam. The analysis is discussed elsewhere[2] and the salient features will be discussed here. The data presented here are from the years 1993-1998 where the event selection has been modified slightly to account for differences in year to year calibrations. Background estimates are based on the original analysis, where the number of $^{12}C(\nu_e, e^-)\ ^{12}N_{GS}$ events is used to estimate the decay at rest flux.

Table 2: LSND Decay at Rest Oscillation Search

Selection	Beam On	Beam Off	ν backgrounds	Excess Signal
$36 < E_e < 60, R > 30$	33	6.2 ± 0.6	3.3 ± 0.7	23.5 ± 5.8
$20 < E_e < 60, R > 30$	70	17.7 ± 1.0	12.8 ± 1.7	39.5 ± 8.8
Fitted Oscillation Probability			$0.33 \pm 0.09 \pm 0.05$	

The reaction that is searched for is the $\bar{\nu}_e p \rightarrow e^+ n$ inverse beta decay reaction. The matrix element for this cross section is indirectly known from the neutron decay time constant. The final state consists of a positron and a neutron. The neutron contributes little to the primary event, however, it rapidly thermalizes with a time constant of 186 μ. The neutron is then captured on the hydrogen in the mineral oil. The result of the capture on the hydrogen is a 2.2 MeV gamma ray which is observed as an event subsequent to the neutrino interaction, correlated in space and in time.

Events are considered in the energy range from 20 MeV to 60 MeV and inside the tank fiducial volume (35cm from the PMT surface inside the tank). The event selection reduces backgrounds from cosmic ray muons, neutrons, and other sources by requiring that the amount of prompt light, and reconstruction of the vertex and direction of the event, be consistent with a positron event. A large sample of Michel decays from stopped cosmic ray muons assures that the efficiency is well determined for this process.

Correlated events over the 18 hit trigger threshold, within the 1000 μs gamma window subsequent to the trigger event, are searched to see if they are consistent with a neutron capture. The correlated events will have the hit distribution characteristic of a 2.2 MeV energy deposition, a time correlation with a 186 μ time constant, and a spatial correlation with an RMS of 74 cm. A likelihood is formed for each future activity from the number of hits, primary and secondary event time difference, and distance between primary and secondary vertices. These distributions are shown in Figure 1 for correlated and uncorrelated gamma samples from cosmic ray data.

Future activities have a likelihood that they were a correlated gamma ray from neutron capture. They also have a likelihood that they were a random background gamma from another source. The ratio of those likelihoods is called R, the correlated-to-uncorrelated gamma likelihood ratio. This ratio is used to discriminate between correlated and uncorrelated gammas in the positron event sample. The data are analyzed in two sets, $R \geq 0$ (no cut on R) and $R > 30$. The requirement of the presence of a correlated neutron capture, $R > 30$, greatly reduces the backgrounds from a number of sources, both beam-related and cosmic ray.

The number of events observed after the event selection is shown in Table 2 for two different sets of selection, a strict selection with $36 < E_e < 60$ MeV and $R > 30$, and a loose selection with $20 < E_e < 60$ MeV and $R > 30$. The energy, angle, and vertex (x,y) distributions for the events satisfying the strict selection is shown in Figures 3,5,and 6. The oscillation probability, defined as the observed number of events divided by the maximum possible number of events in the high Δm^2 limit, is measured by fitting the distribution in R for events in the $20 < E_e < 60$ MeV range. The results of this fit are shown in Figure 2.

The 96-98 period of running was with a higher Z material. Figure 4 shows the energy distribution for $R > 30$ excess events for this running period. The distribution is consistent with the 93-95 running period results and with the neutrino oscillation hypothesis.

The data satisfying the loose selection criteria are binned into positron energy, R, angle with respect to the incident neutrino direction, and distance from the neutrino source. The Poisson likelihood for these binned data are calculated in a model that includes neutrino induced backgrounds, cosmic ray backgrounds, and oscillation events. The oscillation events are taken to be dependent on two parameters, Δm^2 and $sin^2 2\theta$, in the usual form

$$P_{osc} = sin^2 2\theta \; sin^2(1.27 \Delta m^2 L / E_\nu). \quad (1)$$

The log-likelihood function is then calculated as a function of Δm^2 and $sin^2 2\theta$. Regions bounded by contours of 2.3 and 4.5 (90 and 99 percent) units from the peak log-likelihood value, indicating favored regions in the (Δm^2,$sin^2 2\theta$) parameter space, are calculated. Figure 7 shows regions that are a logical OR of a set of regions made by varying systematic errors.

5.2 $\nu_\mu \to \nu_e$ Ocillations

The $\nu_\mu \to \nu_e$ search uses the ν_μ flux from pion decay in flight and searches for $^{12}C(\nu_e, e^-)\ ^{12}N$ events at a level higher than expected from normal processes. The analysis is described in detail in prior publications[3] and is outlined here. The $\nu_\mu \to \nu_e$ relies on the suppression of $\bar{\nu}_e$ in the initial neutrino beam. The data presented here are from the years 1993-1995.

The pion decay-in-flight flux is calculated in the same program that yields the decay-at-rest flux, where good agreement is achieved with the number of observed $^{12}C(\nu_e, e^-)\ ^{12}N$ events. It is checked by the measured number of $^{12}C(\nu_\mu, \mu^-)\ ^{12}N_{GS}$ events observed. That method is statistically limited with an error of around 15 percent, but the method is more reliable than the inclusive $^{12}C(\nu_\mu, \mu^-)\ ^{12}N$ events where the cross section is not known well.

The $^{12}C(\nu_e, e^-)\ ^{12}N$ cross section is calculated by using the CRPA model[11]. This model accurately predicts the $^{12}C(\nu_e, e^-)\ ^{12}N$ process at lower energies as discussed above, but, for higher energy ranges, is known to differ from shell model calculation[12]. This discrepancy is a source of uncertainty in the oscillation background estimates. In the present analysis the larger values of theoretically possible are used which give an overestimate of the backgrounds, although the final result is not too sensitive to the assumption.

Events consistent with the $^{12}C(\nu_e, e^-)\ ^{12}N$ process are searched for in the energy range from 60 MeV to 200 MeV and inside the tank fiducial volume (35cm from the PMT surface inside the tank). The events selection reduces backgrounds from cosmic ray muons, neutrons, and other sources by loose requirements that the amount of prompt light, and reconstruction of the vertex and direction of the event, be consistent with $^{12}C(\nu_e, e^-)\ ^{12}N$ event. A more complex likelihood method is then employed to reconstruct the event. The likelihood method both gives a likelihood for the electron hypothesis and gives the amount of Čerenkov light observed in the Čerenkov cone. Both of these are then used to further select electron events. Significant cosmic ray background persists in the event sample even after this selection and the fiducial volume of the selection is reduced further by requiring that events near the wall of the tank are not pointing into the tank.

The results of two independent sets of software analyses are shown in Table 3. The number of observed events, after including systematic and statistical errors, is higher than that predicted by conventional processes. Figures 8 and 9 show the energy distribution for events that satisfy either analysis along with the predicted signal and background levels.

The chance for a fluctuation to have produced this effect is less than 2 percent. This, in combination with the decay-at-rest result, strongly suggest an unexplained source of electron or positron like events. A confidence region calculation was performed to check the consistency of the $\nu_\mu \to \nu_e$ result with the $\bar{\nu}_\mu \to \bar{\nu}_e$ result. The regions for the two analysis, shown in Figure 10 overlap which shows that the two results can be explained by a single neutrino oscillation hypothesis.

6 Conclusion

The LSND experiment has observed anomalous signals in the $\bar{\nu}_e$ and ν_e channels which are consistent with the hypothesis of neutrino flavor oscillations. In order to demonstrate the the signal is due to neutrino flavor oscillations, a follow-on experiment is necessary which is capable of observing the quantum mechanical phase dependence of the oscillation on L/E. Such an experiment has been proposed and approved at the Fermi National Laboratory, the Booster Neutrino Experiment [13] (BooNE). This experiment will use the rapid cycling 8 GeV proton booster synchrotron at Fermilab to generate a high flux neutrino beam from focussed pions that decay in flight. The experiment will have a sensitivity an order of magnitude greater than LSND and will be able to measure the Δm^2 parameter of the

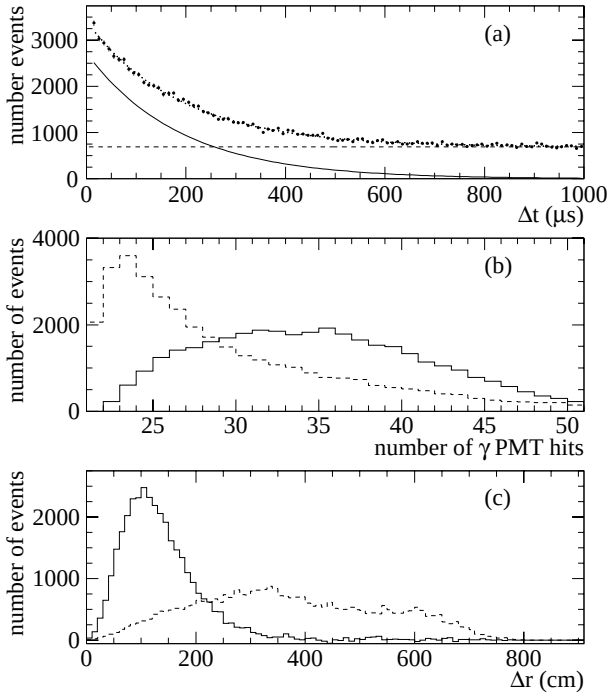

Figure 1: Associated γ distributions for (a) time, (b) PMT hits, and (c) distance distributions for associated (solid) and accidental (dashed) γs.

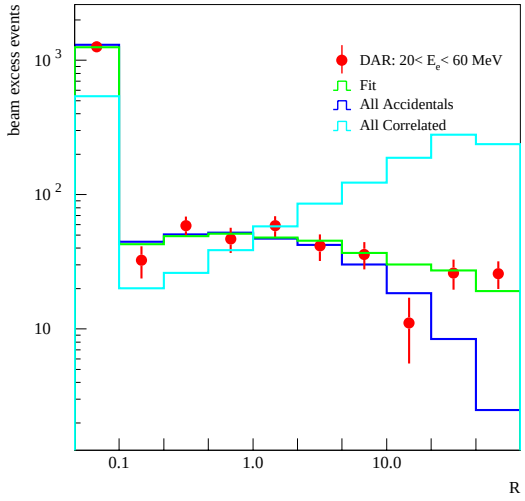

Figure 2: The R distribution, beam on minus beam off excess, for events that have energies in the range $20 < E_e < 60$ MeV. Shown in the figure are the best fit to the data together with the expectations for uncorrelated and correlated γs.

Table 3: LSND Decay in Flight Oscillation Search

Selection	Beam On(Off)	Cosmic events	ν events	Excess Signal	Eff.	Oscillation Prob.
Analysis A	23(114)	8.0 ± 0.7	4.5 ± 0.9	10.5 ± 4.9	0.084	$(2.9 \pm 1.4) \times 10^{-3}$
Analysis B	25(92)	6.4 ± 8.5	8.5 ± 1.7	10.1 ± 5.3	0.138	$(1.7 \pm 0.9) \times 10^{-3}$

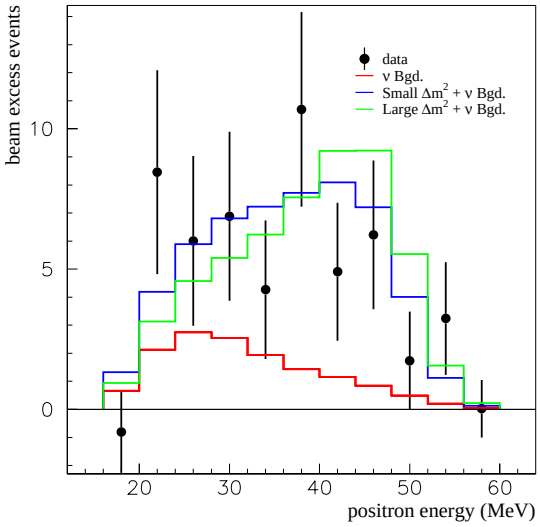

Figure 3: The energy distribution for events with $R > 30$. Shown in the figure are the beam-excess data, estimated neutrino background, expected distribution for neutrino oscillations at large Δm^2 plus estimated neutrino background, and expected distribution for neutrino oscillations at small Δm^2 plus estimated neutrino background.

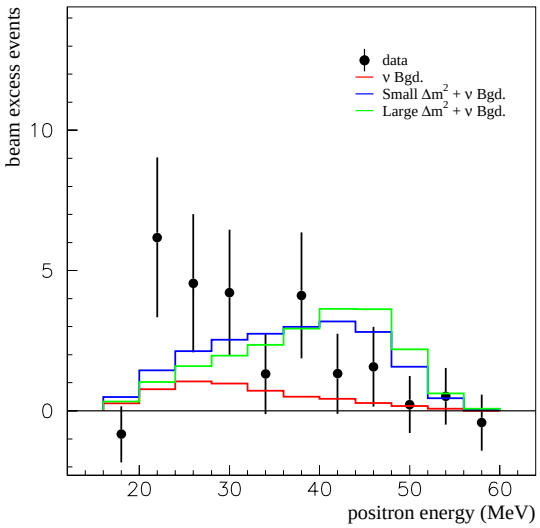

Figure 4: The energy distribution for events with $R > 30$ for the 96-98 running period.

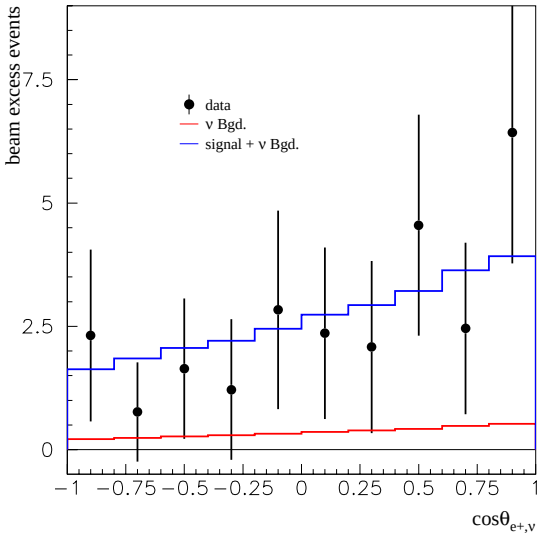

Figure 5: The $\cos\theta_\nu$ distribution for events with $R > 30$ and $36 < E < 60$ MeV, where $\cos\theta_\nu$ is the angle between the neutrino direction and the reconstructed positron direction.

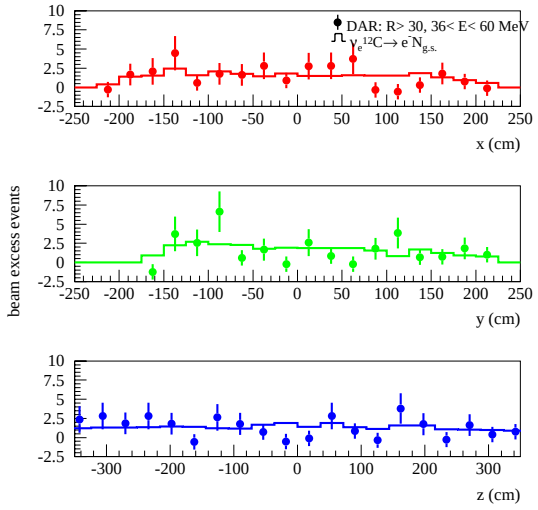

Figure 6: The spatial distributions for events with $R > 30$ and $36 < E < 60$ MeV.

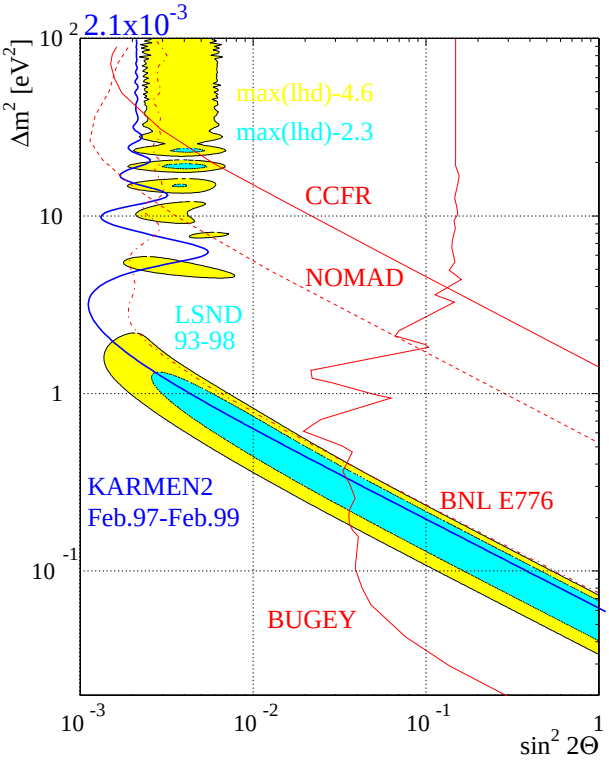

Figure 7: Plot of the LSND Δm^2 *vs* $\sin^2 2\theta$ favored regions. They correspond to 90% and 99% likelihood regions after the inclusion of the effects of systematic errors. Also shown are 90% C.L. limits from KARMEN1 at ISIS, E776 at BNL, the Bugey reactor experiment, the CCFR experiment at FNAL, and the NOMAD experiment at CERN.

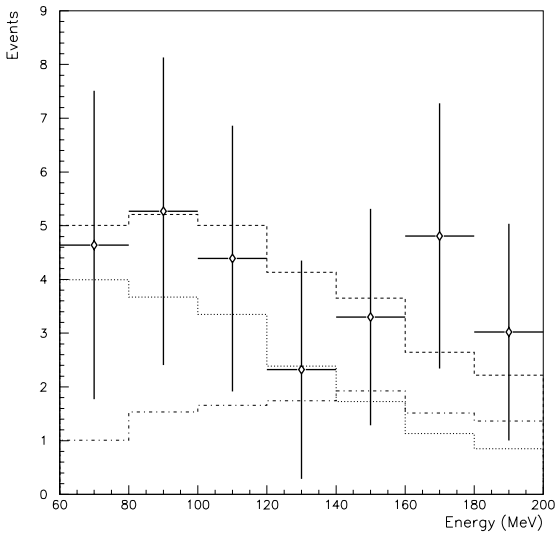

Figure 8: The energy distribution for the final beam-excess decay-in-flight events. The expectation for backgrounds (dot-dashed histogram), the oscillation signal for most likely values of Δm^2 (dotted histogram), and the sum of the two (dashed histogram) are shown.

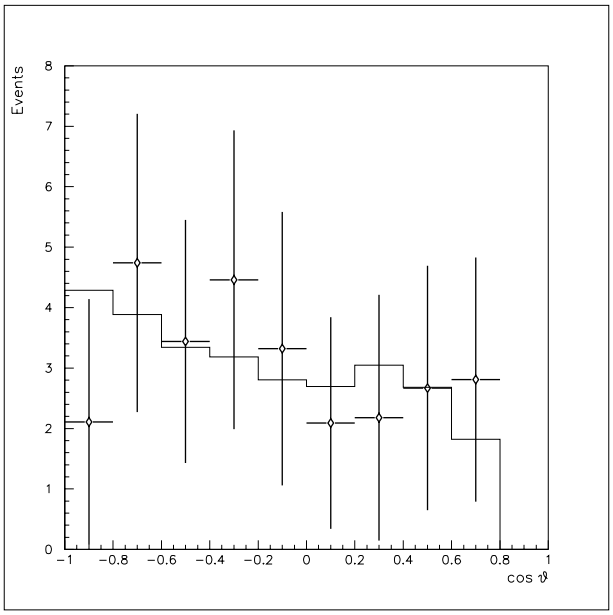

Figure 9: The angular distribution for the final beam-excess decay-in-flight events. The expectation for neutrino background and an oscillation signal at most likely values of Δm^2 (solid histogram) is shown.

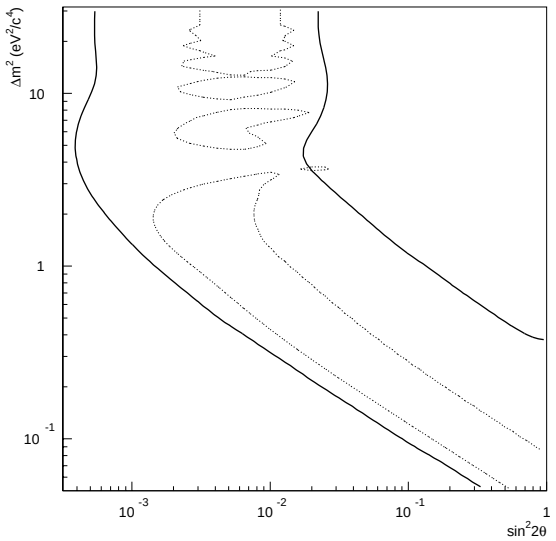

Figure 10: The 95% confidence region for $\nu_\mu \to \nu_e$ oscillations (solid curve) along with the favored regions for $\bar{\nu}_\mu \to \bar{\nu}_e$ oscillations (dotted curve).

oscillations if they are occurring.

1. The LSND Collaboration presently consists of the following people and institutions: E. D. Church, I. Stancu, W. Strossman, G.J. VanDalen (Univ. of California, Riverside); W. Vernon (Univ. of California, San Diego); D.O. Caldwell, S. Yellin (Univ. of California, Santa Barbara); D. Smith (Embry-Riddle Aeronautical Univ.); R.L. Burman, J.B. Donahue, G.T. Garvey, W.C. Louis, G.B. Mills, V. Sandberg, R. Tayloe, D.H. White (Los Alamos National Laboratory); R. Imlay, H.J. Kim, A. Malik, W. Metcalf, M.K. Sung, N. Wadia (Louisiana State Univ.): K. Johnston (Louisiana Tech Univ.); A. Fazely, R.M. Gunasingha (Southern Univ); L.B. Auerbach, R. Majkic (Temple Univ.).
2. C. Athanassopoulos *et al.*, *Phys. Rev. C* **54**, 2685 (1996); C. Athanassopoulos *et al.*, *Phys. Rev. Lett.* **77**, 3082 (1996).
3. C. Athanassopoulos *et al.*, *Phys. Rev. Lett.* **81**, 1774 (1998); C. Athanassopoulos *et al.*, *Phys. Rev. C* **58**, 2489 (1998).
4. R.L. Burman, M.E. Potter, and E.S. Smith, *Nucl. Instrum. Methods A* **291**, 621 (1990); R.L. Burman, A.C. Dodd, and P. Plischke, *Nucl. Instrum. Methods in Phys. Res. A* **368**, 416 (1996).
5. C. Athanassopoulos *et al.*, *Nucl. Instrum. Methods A* **388**, 149 (1997).
6. R.A. Reeder *et al.*, *Nucl. Instrum. Methods A* **334**, 353 (1993).
7. J.J. Napolitano *et al.*, *Nucl. Instrum. Methods A* **274**, 152 (1989).
8. C. Athanassopoulos *et al.*, *Physical Review C* **55**, 2078 (1997).
9. C. Athanassopoulos *et al.*, *Physical Review C* **56**, 2806 (1997).
10. E. Kolbe, K. Langanke, and F.K. Thielemann, and P. Vogel, *Phys. Rev. C* **52**, 3437 (1995).
11. E. Kolbe, K. Langanke, and S. Krewald, *Phys. Rev. C* **49**, 1122 (1994).
12. A.C. Hayes, *Elevier Preprint*, (1998), private communication.
13. E. Church *et al.*, "A proposal for an experiment to measure $\nu_\mu \to \nu_e$ oscillations and ν_μ disappearance at the Fermilab Booster: BooNE", LA-UR-98-352, Fermilab experiment 898.